The Effect of Local Fiber Model On Population Studies

James G. Malcolm Marek Kubicki Martha E. Shenton Yogesh Rathi

Psychiatry Neuroimaging Laboratory, Harvard Medical School, Boston, MA
VA Boston Healthcare System, Brockton Division, Brockton, MA

Abstract. Diffusion tensor imaging has made it possible to evaluate the organization and coherence of white matter fiber tracts. Hence, it has been used in many population studies, most notably, to find abnormalities in schizophrenia. To date, most population studies analyzing fiber tracts have used a single tensor as the local fiber model. While robust, this model is known to be a poor fit in regions of crossing or branching pathways. Nevertheless, the effect of using better alternative models on population studies has not been studied. The goal of this paper is to compare white matter abnormalities as revealed by two-tensor and single-tensor models. To this end, we compare three different regions of the brain from two populations: schizophrenics and normal controls. Preliminary results demonstrate that regions with significant statistical difference indicated using one-tensor model do not necessarily match those using the two-tensor model and vice-versa. We demonstrate this effect using various tensor measures.

1 Introduction

Diffusion tensor imaging (DTI) has become an established tool for investigating tissue structure, and many studies have used it to understand the effects of aging or disease. Using this imaging technique, neuroscientists wish to ask how regions of tissue compare or how well-defined various connections may be. For example, several DTI studies have indicated a disturbance in connectivity between different brain regions, rather than abnormalities within any specific region as responsible for the cognitive dysfunctions observed in schizophrenia [1]. For such studies, the quality of the results depends on the accuracy of the underlying model.

The most common local fiber model used in population studies is a single diffusion tensor which provides a Gaussian estimate of diffusion orientation and strength. While robust, this model can be inadequate in cases of mixed fiber presence or more complex orientations, and so various alternatives have been introduced including mixture models [2,3,4,5] as well as nonparametric approaches [3,6,7,8,9]. Probabilistic techniques have also been developed in connectivity studies [10,11].

Despite this wide selection of available models, nearly all population studies thus far have been based on the single-tensor model, and as such it is important to examine the limits of this model and potential impact this has. To start, some works have focused on the effects of noise and acquisition schemes and have found nontrivial effects on estimated fractional anisotropy (FA) and other quantities [12,13,14]. Beyond such factors, it is known that in regions containing crossing or fanning pathways the single-tensor model itself provides a poor fit that results in lower FA [15,3]. It is estimated that

as much as one third of white matter may contain such putative fiber populations [11]. It is here that this present study focuses.

In forming studies, there are several approaches for comparing patient populations. For example, voxel-based studies examine tissue characteristics in regions of interest [16]. In contrast, tract-based studies incorporate the results of tractography to use fiber pathways as the frame of reference [17,18], and several studies have demonstrated the importance of taking into account local fluctuations in estimated diffusion [19,20,21,22,23].

To date, many studies have focused on schizophrenia, but the findings vary. For example, the review by Kubicki *et al*. [1] cites one voxel-based study where the genu of the corpus callosum has significant differences and another that finds nothing. A recent tract-based study showed statistical differences not only in the genu of the corpus callosum but also in regions known to have fiber crossings and branchings [22]. The question then arises, as to whether the same effect can be seen by better models able to resolve crossings and branchings? Is the population difference simply a result of poor modeling? We seek to answer such questions in this present work.

2 Our contributions

In this paper, we make a first attempt towards confirming or creating doubts regarding the results reported using the single-tensor model. Specifically, we compare various tensor metrics as estimated using two-tensor and single-tensor models on a number of fiber tracts generated using our recently proposed method for deterministic two-tensor tractography [24]. Hence we are continuing this work with a focus on how such techniques will begin affecting clinical studies. It is important to note that this is the first time the same population study has been performed using two different underlying models.

We begin with synthetic experiments to examine the difference in reported FA using single- and two-tensor models. We find that the single-tensor model consistently underestimates the FA by as much as 30% in crossing regions, a difference considered statistically significant in many studies. Then, we look at connections between three different cortical regions of the brain and show that statistical group differences reported using the single-tensor model do not necessarily show differences using the two-tensor model and vice-versa. Specifically, the regions known to have branchings and crossings reports significant differences in the single tensor study, but not in the two-tensor study, and conversely, certain regions which show subtle abnormalities using the two-tensor method are lost in the single-tensor model. Thus, model error may have contributed to the statistical differences found in previous DTI studies.

3 Method

In this paper, we form a tract-based study using the two-tensor tractography method described in [24], and we compare this against the results from a single-tensor model. Section 3.1 provides the necessary background on modeling the measured signal using tensors and defines the specific two-fiber model employed in this study. Section 3.2 looks at the seed regions and the resulting fibers connecting each hemisphere and finally how these fibers are compared within a tract-based coordinate system.

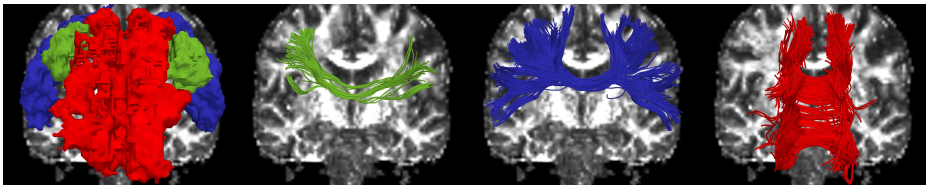

(a) Seed regions **(b)** *Caudalmiddle frontal* **(c)** *Precentral* **(d)** *Superiorfrontal*

Fig. 1: For each patient, we seed in three different cortical regions and select only those fibers that connect the hemispheres.

3.1 Modeling local fiber orientations

In diffusion weighted imaging, image contrast is related to the strength of water diffusion, and our goal is to accurately relate these signals to an underlying model of putative fibers. At each image voxel, diffusion is measured along a set of distinct gradients, $\mathbf{u}_1, ..., \mathbf{u}_m \in \mathbb{S}^3$ (on the unit sphere), producing the corresponding signal, $\mathbf{s} = [\, s_1, ..., s_m \,]^T \in \mathbb{R}^m$. The single-tensor signal model is expressed as, $s_i = s_0 e^{-b\mathbf{u}_i^T D \mathbf{u}_i}$, where s_0 is the baseline signal intensity, b is an acquisition-specific constant, and D is the tensor representing a diffusion pattern.

In this study, our two-tensor model is a mixture of two equally-weighted components. This choice is guided by several previous studies which found two-component models to be superior compared with single-component models at $b = 1000$ [3,4,11]. As demonstrated in [24], while assuming equally-weighted compartments limits the flexibility of the model, we have found that this allows a robust estimate of a reduced set of parameters and produces sufficient tractography (see Fig. 1) beyond that obtainable with the single-tensor model. An additional assumption is that the shape of each tensor is ellipsoidal, *i.e.* there is one dominant principal diffusion direction $\mathbf{m}$ with eigenvalue λ_1 and the remaining orthonormal directions have equal eigenvalues $\lambda_2 = \lambda_3$ (as in [4]). These assumptions leave us with the following two-tensor signal model:

$$s_i = \tfrac{s_0}{2} e^{-b\mathbf{u}_i^T D_1 \mathbf{u}_i} + \tfrac{s_0}{2} e^{-b\mathbf{u}_i^T D_2 \mathbf{u}_i}, \tag{1}$$

where tensors D_1, D_2 are each expressible as $D = \lambda_1 \mathbf{m}\mathbf{m}^T + \lambda_2 \left(\mathbf{p}\mathbf{p}^T + \mathbf{q}\mathbf{q}^T\right)$, with $\mathbf{m}, \mathbf{p}, \mathbf{q} \in \mathbb{S}^3$ forming an orthonormal basis aligned to the principal diffusion direction $\mathbf{m}$. The free model parameters are then $\mathbf{m}_1$, λ_{11}, λ_{21}, $\mathbf{m}_2$, λ_{12}, and λ_{22}.

Several scalar measures have been proposed for quantifying various aspects of tensors, and in this study we focus on fractional anisotropy (FA), trace, and the ratio between eigenvalues (λ_2/λ_1). Since these measures are defined for the single-tensor model, when computing their value on the two-tensor model, we record the value from the tensor most aligned with the local fiber tangent.

3.2 Tractography and fiber comparison

For each patient, we have manually delineated cortical regions from which we choose three regions covering the frontal and parietal lobe. For one patient, Fig. 1 shows these

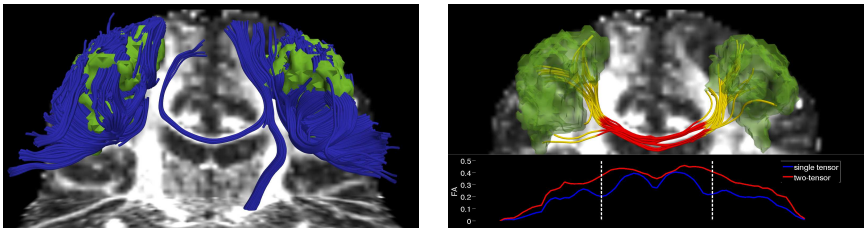

(a) Single-tensor. **(b)** Two-tensor and FA curves

Fig. 2: Single-tensor tractography finds no connections. Two-tensor passes through the region of crossing *(red/yellow boundary)*. FA curves show drop in single-tensor FA *(blue)* in this region *(indicated by dashed white line)*.

seed regions and the resulting fibers that connect each hemisphere. Specifically, the regions are the *superiorfrontal*, *precentral*, and *caudalmiddle frontal*.

We followed the deterministic fiber tracking procedure in [24]. We begin by seeding each algorithm several times in each voxel of the seed regions. To explore branchings found using the proposed technique, we considered a component to be branching if it was separated from the primary component by less than 40° with FA$\geq$0.15. We terminated fibers when either the general fractional anisotropy [3] of the estimated signal fell below 0.1 or the primary component FA fell below 0.15. While such parameters are heuristic in nature and could be examined in their own right, we found the resulting tractography to be sufficient for the purposes of this work.

It is known that single-tensor streamline tractography is only able to trace out the dominant pathways forming the U-shaped callosal radiation, so previous tract-based studies looking at the corpus callosum have been restricted to only studying portions of the corpus radiata, typically focusing on the splenum and genu [19,20,23,22]. One of the main advantages of using the multi-tensor filtering approach in [24] is that it is one of the few techniques capable of following, not only these dominate pathways, but also the transcallosal pathways out to the lateral gyri. For example, Fig. 2a shows that for the *caudalmiddle frontal* region, using single-tensor tractography leads to nearly all fibers looping back into another sulci instead of finding any connection to the opposite hemisphere. In contrast, Fig. 2b demonstrates that the filtered two-tensor approach finds several connecting pathways. Therefore, this is the first attempt at tract-oriented analysis along such pathways.

Since this study focuses on comparing fiber models, we simply perform direct single-tensor estimation at the same locations as we have two-tensor estimates, thus providing an exact correspondence for averaging within each patient. Fig. 3 shows the *precentral* region and colors the same fibers with FA intensity to show the relative FA differences reported by either model.

After performing tractography, we placed fibers from each patient within a common coordinate system by registering the seed regions to a template. Each seed region was registered separately. The mid-sagittal plane was automatically determined and provided a common reference point for each fiber as it passed through the corpus callosum. From this reference point, we record arc-length moving outward to the cortical

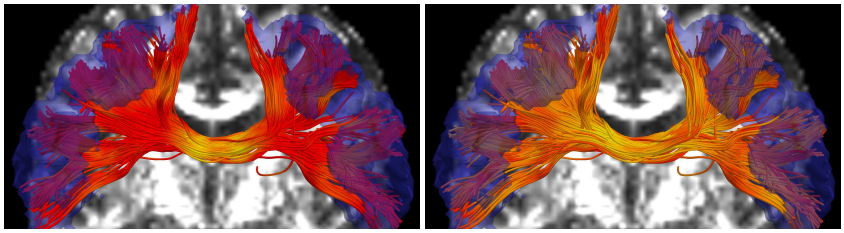

(a) Single-tensor FA. **(b)** Two-tensor FA.

Fig. 3: Two-tensor fibers overlayed with FA intensity using both models *(red to yellow is low to high)*. Both methods show high FA in the corpus callosum but single-tensor FA drops as fibers enter the gray matter.

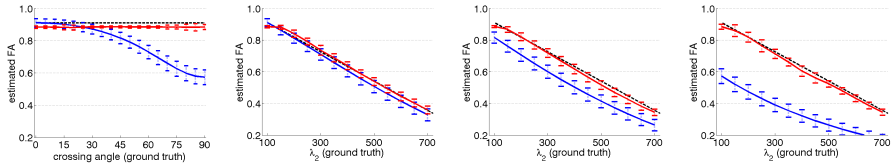

(a) Fixed eigenvalues **(b)** No crossing **(c)** Crossing at 45° **(d)** Crossing at 90°

Fig. 4: Estimated fractional anisotropy (FA) using single-tensor *(blue)* and two-tensor *(red)* models on synthetic data with known FA *(dashed black)*. The two-tensor model accurately captures the FA across a wide range of angles and eigenvalues.

regions. The fibers of each patient being registered with a template and having an origin, we can plot the various scalar tensor measures along this arc-length as in other tract-based studies. For example, Fig. 2b shows FA as a function of arc-length for the *caudalmiddle frontal* region using the single-tensor model *(blue)* and two-tensor model *(red)*. Since the single- and two-tensor estimates line up exactly, any correspondence error is confined to the matching within fiber bundles and among patients–not across models which was our focus here. As in [21,22], statistical significance was tested as a function of arc-length.

4 Results

We first use experiments with synthetic data to validate our technique against ground truth. By varying crossing angle or eigenvalues used to construct voxels, we confirm that our approach accurately estimates the fractional anisotropy while using the single-tensor model can under-estimate FA by as much as 30-40%. (Section 4.1). Then, we examine our real dataset to demonstrate the different results reported using either model (Section 4.2).

4.1 Synthetic validation

Following the experimental method of generating synthetic data found in [8,6], we generated synthetic MR signals according to Eq. 1 using eigenvalues determined from out *in vivo* data. We use 81 gradient directions uniformly spread on the hemisphere and Ri-

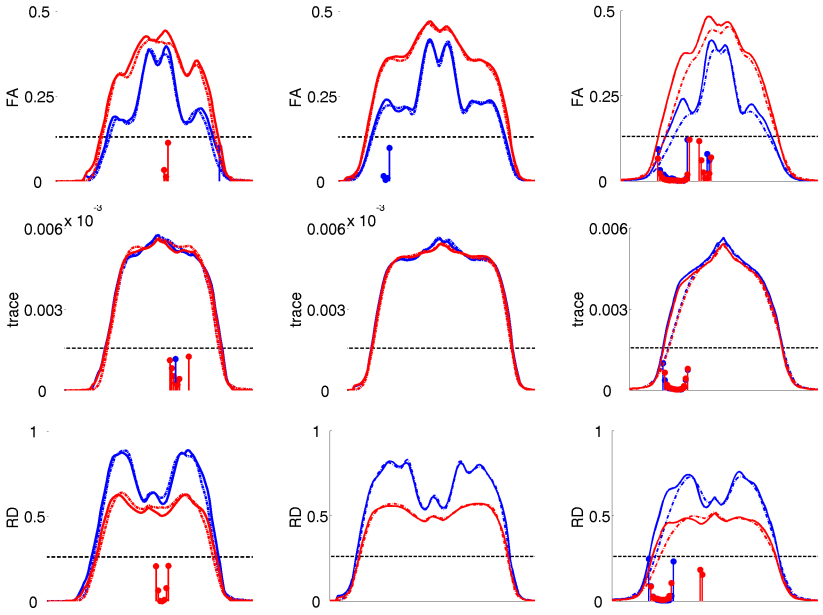

(a) *Caudalmiddle frontal* **(b)** *Precentral* **(c)** *Superiorfrontal*

Fig. 5: Average of various tensor metrics as a function of arc-length using single-tensor *(blue)* and two-tensor *(red)* models comparing normal patients *(solid lines)* with schizophrenic patients *(dotted lines)*. Rows show FA, trace, eigenvalue ratio. Areas of statistical significance are indicated along the bottom *(black dashes indicate 95% confidence)*. While each metric generally indicates the same area of significance *(looking down columns*), the areas of significance vary with each model *(comparing red and blue)* .

cian noise (SNR $\approx$ 10 dB) based on the unweighted signal. Using these we constructed a set of two-dimensional fields through which to navigate while estimating FA.

Fig. 4 shows the resulting FA estimates using direct single-tensor estimation *(blue)* and filtered two-tensor estimation *(red)*. As expected, Fig. 4a demonstrates that crossing regions can lead to single-tensor FA estimates as much as 0.3 lower than expected. In Fig. 4b we look at both techniques accurately estimating the FA of a single tensor as we adjust the second eigenvalue (λ_2 in Eq. 1). However, Fig. 4c and 4d demonstrate a consistent drop in FA under the same range of eigenvalues. This experiment demonstrates that we may expect as much as 0.2 to 0.3 drop in FA in regions of crossing and branching.

4.2 *In vivo* model comparison

We tested our approach on a human brain scans using a 3-Tesla magnet to collect 51 diffusion weighted images on the hemisphere at a voxel size of $1.66 \times 1.66 \times 1.7\,\mathrm{mm}^3$ and with $b = 900\,\mathrm{s/mm}^2$ in addition to eight baseline scans. Included in this study are 17 normal controls and 22 schizophrenics; however, since not connecting fibers were

not found in all patients for all regions, not all patients were represented in each regional group. Below are the sizes for each region and group.

	Caudalmiddle frontal	*Precentral*	*Superiorfrontal*
Normals	16	17	8
Schizophrenics	20	22	17

For each region and patient group, Fig. 5 shows the resulting average curves using the single-tensor *(blue)* and two-tensor *(red)* models. Along the bottom of each plot we indicate local regions of statistical significance between groups. In Fig. 5a we see that the two-tensor model detected a region of significance across all three measures whereas the single-tensor model found only one small portion of that in the trace. As Fig. 2b indicates, this a region known to contain branching and crossing, hence the single-tensor FA drop. Thus, we suspect that the single-tensor was unable to provide a tight enough fit in this region to detect the difference found using the two-tensor model. In Fig. 5b we see that the single-tensor model found a slight area again in a region of known branching, yet the two-tensor model found nothing. In Fig. 5c we see the most reported differences and further we see those differences reported using both models. We note that these differences may in part be due to the relative size of each population supporting this region. In summary, among these three regions, we see areas where each model either confirmed or denied the findings of the other.

5 Conclusion

There are many challenges in building automatic frameworks for detecting population differences. By repeating the same tract-based study and changing only the model, we have demonstrated that the ultimate findings may vary. Specifically, our results indicate that some areas reported as significant using the single-tensor model may in fact be due to poor modeling at branchings or crossings.

While our results are preliminary, we believe that exploring both alternative models and methods of reconstructing pathways will provide more accurate and comprehensive information about neural pathways and ultimately enhance non-invasive diagnosis and treatment of brain disease.

Considering future work, we expect that further model discrepancies may be revealed with more accurate fiber and patient correspondences [21,22] or functional representations [23].

References

1. Kubicki, M., McCarley, R., Westin, C.F., Park, H.J., Maier, S., Kikinis, R., Jolesz, F., Shenton, M.: A review of diffusion tensor imaging studies in schizophrenia. J. of Psychiatric Research **41** (2007) 15–30
2. Alexander, A., Hasan, K., Tsuruda, J., Parker, D.: Analysis of partial volume effects in diffusion-tensor MRI. Magnetic Resonance in Medicine **45** (2001) 770–780
3. Tuch, D., Reese, T., Wiegell, M., Makris, N., Belliveau, J., Wedeen, V.: High angular resolution diffusion imaging reveals intravoxel white matter fiber heterogeneity. Magnetic Resonance in Medicine **48** (2002) 577–582
4. Peled, S., Friman, O., Jolesz, F., Westin, C.F.: Geometrically constrained two-tensor model for crossing tracts in DWI. Magnetic Resonance in Medicine **24**(9) (2006) 1263–1270

5. Hall, M., Alexander, D.: Agreement and disagreement in two models of synthetic diffusion MR data. In: Int. Symp. on Magnetic Resonance in Medicine (ISMRM). (2008) 1780
6. Descoteaux, M., Deriche, R., Anwander, A.: Deterministic and probabilistic Q-ball tractography: from diffusion to sharp fiber distributions. Technical Report 6273, INRIA (2007)
7. Jansons, K., Alexander, D.: Persistent angular structure: New insights from diffusion MRI data. Inverse Problems **19** (2003) 1031–1046
8. Tournier, J.D., Calamante, F., Gadian, D., Connelly, A.: Direct estimation of the fiber orientation density function from diffusion-weighted MRI data using spherical deconvolution. NeuroImage **23** (2004) 1176–1185
9. Jian, B., Vemuri, B.: A unified computational framework for deconvolution to reconstruct multiple fibers from diffusion weighted MRI. IEEE Trans. on Med. Imag. **26**(11) (2007) 1464–1471
10. Parker, G., Alexander, D.: Probabilistic Monte Carlo based mapping of cerebral connections utilizing whole-brain crossing fiber information. In: Information Processing in Medical Imaging (IPMI). (2003) 684–696
11. Behrens, T., Johansen-Berg, H., Jbabdi, S., Rushworth, M., Woolrich, M.: Probabilistic diffusion tractography with multiple fibre orientations: What can we gain? NeuroImage **34** (2007) 144–155
12. Basser, P., Pajevic, S.: Statistical artifacts in diffusion tensor MRI (DT-MRI) caused by background noise. Magnetic Resonance in Medicine **44**(1) (2000) 41–50
13. Jones, D., Basser, P.: Squashing peanuts and smashing pumpkins: How noise distorts diffusion-weighted MR data. Magnetic Resonance in Medicine **52**(5) (2004) 979–993
14. Goodlett, C., Fletcher, P., Lin, W., Gerig, G.: Quantification of measurement error in DTI: Theoretical predictions and validation. In: Medical Image Computing and Computer Assisted Intervention (MICCAI). (2007) 10–17
15. Alexander, D., Barker, G., Arridge, S.: Detection and modeling of non-Gaussian apparent diffusion coefficient profiles in human brain data. Magnetic Resonance in Medicine **48** (2002) 331–340
16. Ashburner, J., Friston, K.: Voxel-based morphometry–The methods. NeuroImage **11**(6) (2000) 805–821
17. Ding, Z., Gore, J., Anderson, A.: Classification and quantification of neuronal fiber pathways using diffusion tensor MRI. Magnetic Resonance in Medicine **49** (2003) 716–721
18. Smith, S., Jenkinson, M., Johansen-Berg, H., Rueckert, D., Mackay, T., Watkins, K., Ciccarelli, O., Cader, M., Matthews, P., Behrens, T.: Tract-based spatial statistics: Voxelwise analysis of multi-subject diffusion data. NeuroImage **31** (2006) 1487–1505
19. Corouge, I., Fletcher, P., Joshi, S., Gouttard, S., Gerig, G.: Fiber tract-oriented statistics for quantitative diffusion tensor MRI analysis. Medical Image Analysis **10**(5) (2006) 786–798
20. Fletcher, P., Tao, R., Joeng, W., Whitaker, R.: A volumetric approach to quantifying region-to-region white matter connectivity in diffusion tensor MRI. In: Information Processing in Medical Imaging (IPMI). (2007) 346–358
21. O'Donnel, L., Westin, C.F., Golby, A.: Tract-based morphometry. In: Medical Image Computing and Computer Assisted Intervention (MICCAI). (2007) 161–168
22. Maddah, M., Kubicki, M., Wells, W., Westin, C.F., Shenton, M., Grimson, W.: Findings in schizophrenia by tract-oriented DT-MRI analysis. In: Medical Image Computing and Computer Assisted Intervention (MICCAI). (2008)
23. Goodlett, C., Fletcher, P., Gilmore, J., Gerig, G.: Group statistics of DTI fiber bundles using spatial functions of tensor measures. In: Medical Image Computing and Computer Assisted Intervention (MICCAI). (2008) 1068–1075
24. Malcolm, J., Shenton, M., Rathi, Y.: Neural tractography using an unscented Kalman filter. In: Information Processing in Medical Imaging (IPMI). (2009) 126–138